Landslides (2019) 16:1367–1374
DOI 10.1007/s10346-019-01188-6
Received: 12 January 2019
Accepted: 25 April 2019
Published online: 15 May 2019

Lianheng Zhao · Dejian Li · Hanhua Tan · Xiao Cheng · Shi Zuo

Characteristics of failure area and failure mechanism of a bedding rockslide in Libo County, Guizhou, China

Abstract Owing to the continuous rainfall, a bedding rockslide occurred at a construction site on the San-Li highway (Sandu County to Libo County) at 18:05 (UTC+8) on September 23, 2017, in Libo County, Guizhou Province, China. This bedding rockslide caused three deaths, six injuries, and an accumulation zone of approximately 1.8×10^5 m^3 of medium weathered limestone that blocked the main line of the M ramp. To explore the triggering factors of this rockslide, the engineering geological condition, hydrogeological condition, slope excavation scheme, and statistics of rainfall data were investigated based on field investigations and geophysical drilling. The blasting failure of the upper unstable and dangerous rock masses after the bedding rockslide was analyzed. Three instability behaviors characteristics are distinguished: (1) the bedding characteristics of the rock formation and weak interlayer, (2) the steep slope (the largest dip angle being 46°), and (3) the appearance of the free face induced by the slope excavation. The results indicate that the above conditions are objective factors, and continuous rainfall triggers the bedding rockslide. The landslide follows the step-path failure mode.

Keywords Bedding rockslide · Field investigation · Step-path failure mode · Instability mechanism · Slope excavation · Rainfall

Introduction

There are many factors inducing the occurrence of bedding rockslides. For internal factors, most researches focused on the failure mechanisms of weak interlayers (Yin et al. 2011; Tang et al. 2015; Huang et al. 2016; Zhao et al. 2016; Gu et al. 2017; Regmi et al. 2017; Wang et al. 2017; Lin et al. 2018; Xue et al. 2018). For external factors, hydraulic conditions (i.e., rainfall and groundwater) (Zhang et al. 2011, 2016; Li et al. 2016; Ouyang et al. 2017; Cogan et al. 2018; Huang et al. 2018; Lin et al. 2018; Tang et al. 2018; Zhao et al. 2018) and slope excavation (Cen et al. 2017; Ouyang et al. 2017; Lin et al. 2018; Xue et al. 2018) were usually studied.

This study attempts to explore the occurrence process and failure mechanism of the Libo bedding rockslide based on characterizing its failure area. The contributions of geological factors, engineering geological structures, slope excavation, and continuous rainfall towards triggering the landslide are investigated in detail. In addition, the blasting failure of the upper unstable and dangerous rock masses is discussed.

Bedding rockslide background

A bedding rockslide accident occurred at 18:05 (UTC+8) on September 23, 2017, at a construction site on the San-Li highway, in Libo County, Guizhou Province, China (Figs. 1 and 2). This rockslide caused three deaths, six injuries, and an accumulation zone of medium weathered limestone that blocked the main line of the M ramp (MK0+165 ~ MK0+400). The distance from the front edge of the upper unstable and dangerous rock masses area to the route is 140 m. The azimuth of the main sliding direction is approximately 255°. In addition, the length of the landslide body (route direction) is approximately 235 m; the width (sliding direction) is approximately 89.5 m, and the average thickness is approximately 9 m. The volume of the landslide body is approximately 1.8×10^5 m^3.

Geomorphological characteristics

The Libo bedding rockslide was located on the western side of the elliptical massif, and the route is arc-shaped. The right side of the route was a high slope (the maximum elevation of 707.4 m), and the left side of the route was a low embankment (the maximum elevation of 525.3 m). Based on field investigations, the dip angle of the slope ranges from 24° to 46° (Table 1). The scouring action of rainfall and the steep slope increased the likelihood of slope failure.

Geological characteristics

Using the exposed rock masses (Fig. 3), field investigations, and geological survey report, the material composition of the surface soil masses and the underlying bedrock was studied. In addition, no fault structures or new tectonic movements could be found in the proximity of the failure. The rock formation showed a single oblique structure. The attitudes of the rock formation in the main sections of the bedding rockslide are shown in Table 1.

The surface soil mass was a reddish-brown silty clay (Q_4^{dl+el}, the number of strata is 2–32) with low water content ($\omega = 28.6\%$) and high plasticity (the liquid limit "ω_L" is 51%, and the plasticity index "I_p" is 29.8). In addition, it contained a small amount of limestone breccia (the particle size ranging from 2 to 16 mm) and had a certain degree of contamination in the underlying bedrock. The maximum depth of the reddish-brown silty clay was 0.80 m (Fig. 4).

The underlying bedrock was primarily a medium weathered limestone (C_3mp, the number of strata is 7–12). The joints were well developed; the integrity of the rock masses was good, and the rock was hard (the hardness value is 4.3). Joints filled with hard or soft rock masses were rough. There was a mudstone interlayer in the limestone (Fig. 3a). In part position, developed calcites were found along the sliding surface (Fig. 3b). Specific geological information can be determined based on drill holes SLZK44 and SLZK45 (Fig. 4). The integrity of the drill cores was good. Most of rock cores were columnar with a size larger than 10 cm, and the lengths were generally 10–32 cm, though the longest was 42 cm. In addition, a few rock cores were lumpy with a size ranging from 2 to 10 cm, and the lengths were generally 3–8 cm. The rock quality designations were 70% (SLZK44) and 74% (SLZK45).

The bedding characteristics and weak interlayer are the main internal factors triggering bedding rockslides (Yin et al. 2011; Zou 2014; Tang et al. 2015). Based on the geological characteristics of the Libo bedding rockslide, Table 1 shows the bedding

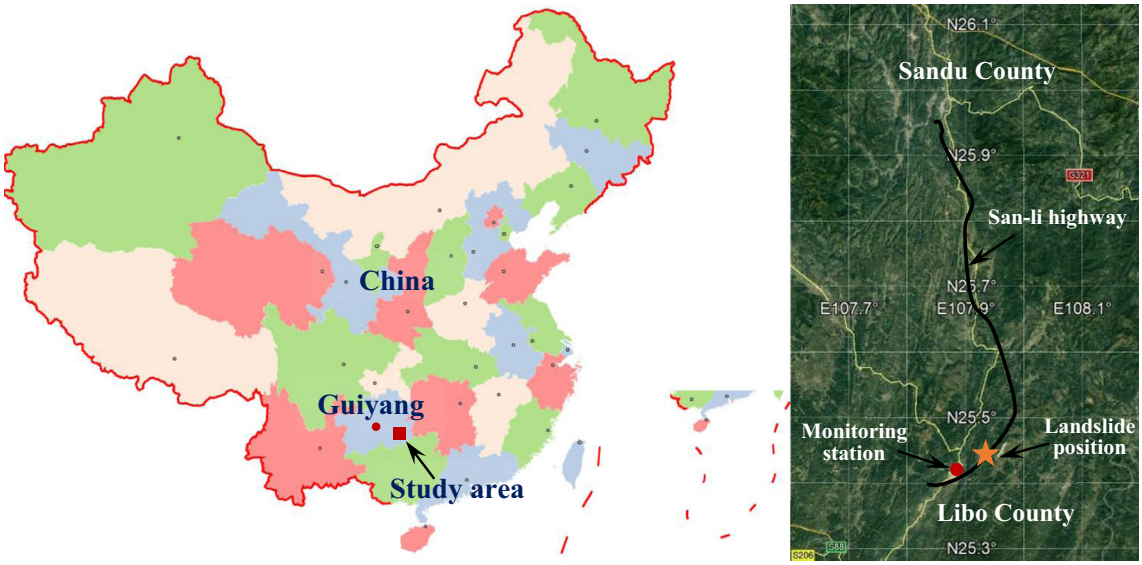

Fig. 1 Landslide location map

characteristics of the rock formation. A weak interlayer was identified by investigating the sliding bed (Fig. 3a), along which a potential sliding surface could be easily developed under these geological conditions. The joints provided room for the development of calcites (Fig. 3b). Through the above analyses, these geological characteristics contributed to high risk of a landslide.

Hydrogeological conditions

The types of groundwater in the landslide area are primarily Quaternary pore water and bedrock fissure water. The Quaternary pore water mainly existed in the residual soil layer and the aquifer is thin. The bedrock fissure water was presented in the fissure. The aqueous characteristics of groundwater were generally weak owing to the limitation of recharge conditions. Before the rockslide, there was a mark of groundwater seepage at the foot of the slope (Fig. 5).

By querying the local climate resources (monitoring station ID is 57,936, in Libo County, Guizhou Province, China), the cumulative rainfall in Libo County in September 2017 was 138.5 mm, and rainfall was relatively frequent (Fig. 6). In September 2017, there were 10 days during which the rainfall exceeded 1 mm, and 7 days during which the rainfall ranged between 0 and 1 mm. In particular, the daily rainfall on September 20 reached 64.3 mm (Fig. 6). The rainfall not only increases the unit weight of the rock masses but also decreases the shear strength of the rock masses and sliding band. In addition, a large amount of rainwater infiltrated into the rock masses of the slope body through preexisting cracks, resulting in a loss in strength of rock masses. Thus, under the action of rainwater, the rock masses were further softened and its shear strength reduced.

Slope excavation

According to the design plan, the slope was to be excavated dividing into five slope grades, and the maximum excavation height is 51.9 m. The stepped-slope excavated mode was adopted: based on Fig. 7, the slope ratios (height: width) corresponding to the first grade to the fifth grade were respectively 1:0.75, 1:0.75, 1:0.75, 1:1, and 1:1. The platform width was 2 m. The former four slope grade heights were all equal to 10 m and the fifth one was 11.9 m. The first grade and fourth grade were reinforced by 8.5-m- and 11.5-m-long anchor rods. In addition, the second grade and third grade were reinforced by 22-m- and 25-m-long anchor cables. In the fifth grade, the shrubs were used for the slope protection. Before the landslide, the anchor rods were constructed in the fourth slope grade. The third slope grade was excavated; however, the anchor cables were not constructed.

Characteristics of failure area

According to field investigations, the failure area is divided into three parts: the upper unstable and dangerous rock masses area (area I), the middle stable sliding bed area (area II), and the lower accumulation zone area (area III) (Fig. 8a). The middle stable sliding bed area (area II) is divided into two sub-regions by a fracture platform with an average thickness of approximately 2 m (Fig. 8a): first-grade sliding bed area (area II-1) and second-grade sliding bed area (area II-2). The shape of the sliding bed indicates that the landslide follows the step-path failure mode (Fig. 8b).

1. The upper unstable and dangerous rock masses area (area I)

This part is located at the top of the slope with a circular tension fracture groove at the lower part. The maximum longitudinal (sliding direction) length is approximately 25 m, and the average thickness is approximately 6 m. The volume of this part is approximately 8000 m^3. Most of this area is covered by plants (Fig. 8a).

2. The middle stable sliding bed area (area II)>

Based on the shape of a middle stable sliding bed, the failure mode of this landslide is not shear failure of the rock bridge along

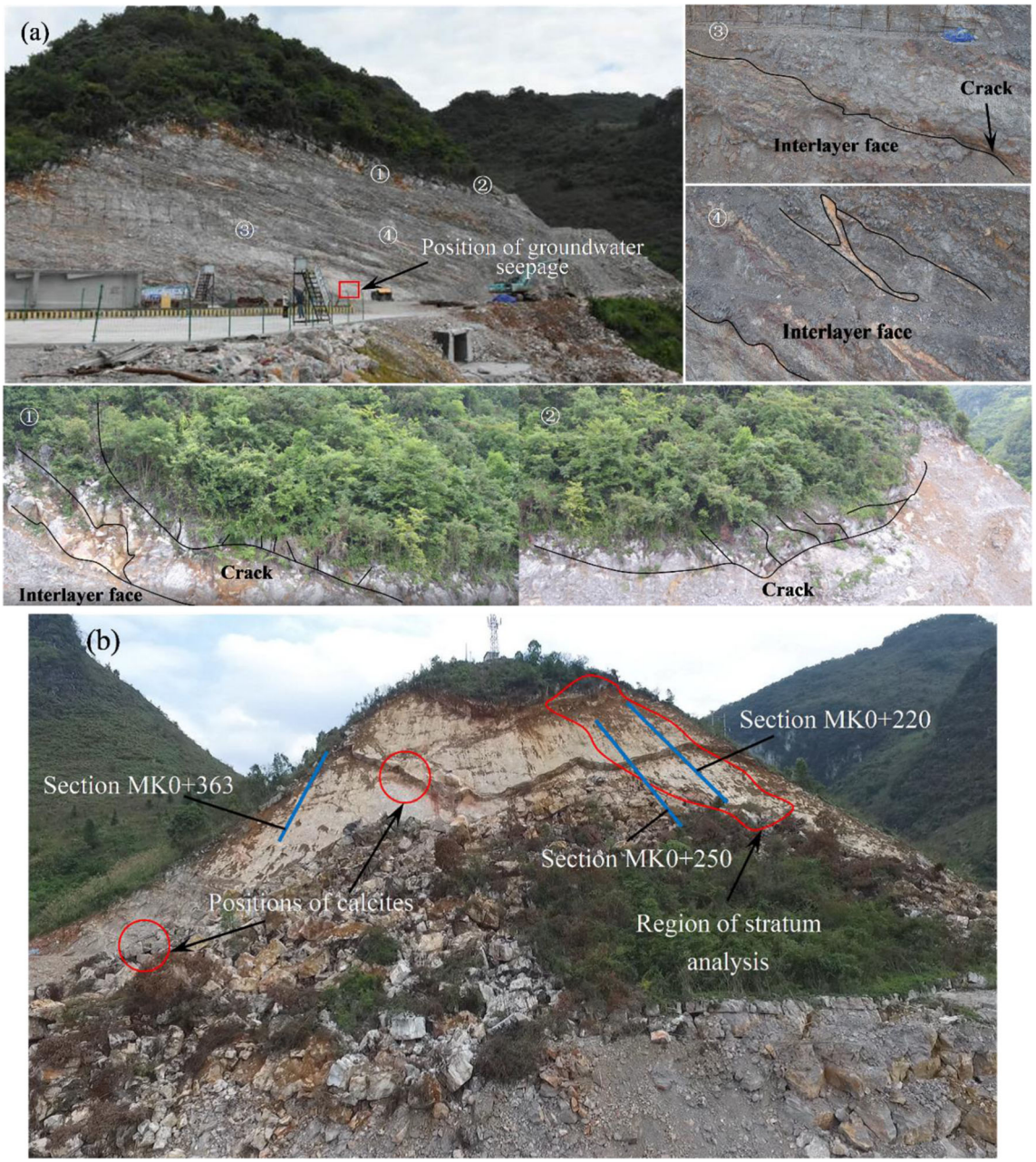

Fig. 2 Slope conditions. **a** Before the landslide; **b** after the landslide

joint surfaces but tensile failure of the rock bridge between adjacent joint surfaces (Fig. 8b). In addition, based on Fig. 8a, before and after the landslide, the red line represented an interface between the sliding surface and the original slope surface on the left and right sides of the sliding bed.

(a) First-grade sliding bed area (area II-1)>

There were sliding groove lines on the left and right sides of area II-1. The sliding bed surface was relatively smooth with several evident slickensides (Fig. 8a). There were also many cracks on the sliding bed surface and a tension crack in the fracture platform (Fig. 8a).

(b) Second-grade sliding bed area (area II-2)>

The sliding bed surface had several evident slickensides and many cracks (Fig. 8a). Small soils and small stones could be seen in part position on the slipping surface. The tension crack cut through under the action of rainfall softening and sliding forces. Finally, the overlying rock masses of the area II-2 slid directly along the joint surface.

3. The lower accumulation zone area (area III)>

This part is located on the roadbed slope and embankment slope (Fig. 8a). The thickness and volume of the accumulation

Fig. 3 The geological conditions of the bedding rockslide. **a** The situations of stratum; **b** the calcites filled in the joints surface

zone are not clear. The length is approximately 260 m and the maximum width is approximately 115 m. The extent is approximately 1.42×10^4 m² in area.

Failure mechanism

Through combining triggering factors, the failure mechanism of the bedding rockslide was analyzed as follows:

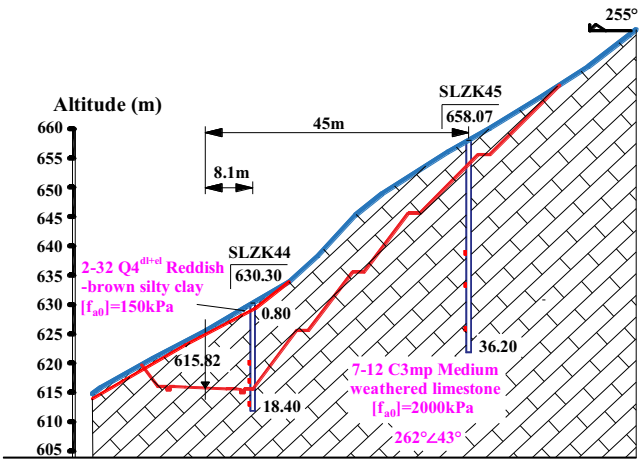

Fig. 4 Cross-section of MK0+220 before the landslide (Q_4^{dl+el} is Quaternary system clinosol and residual. C_3mp is Carboniferous system Ma'ping group. The depth of reddish-brown silty clay is 0.8 m. The depths of the drill holes SLZK44 and SLZK45 are 18.40 m and 36.20 m, respectively)

1. The rock masses were columnar and lumpy containing the multiple groups of structures surfaces. Rainwater infiltrated into the rock masses of the slope through the tension fracture groove and surface fractures of rock masses. The medium weathered limestone belongs to the carboniferous system Ma'ping group. This type of rock is vulnerable to strength reduction induced by water; thus, a sliding band can be easily formed under the action of rainwater and other external forces (Zou 2014). In addition, when the flowing rainwater conveyed carbon dioxide (CO_2) into the rock masses, the calcium

Fig. 5 Groundwater seepage at the foot of the slope

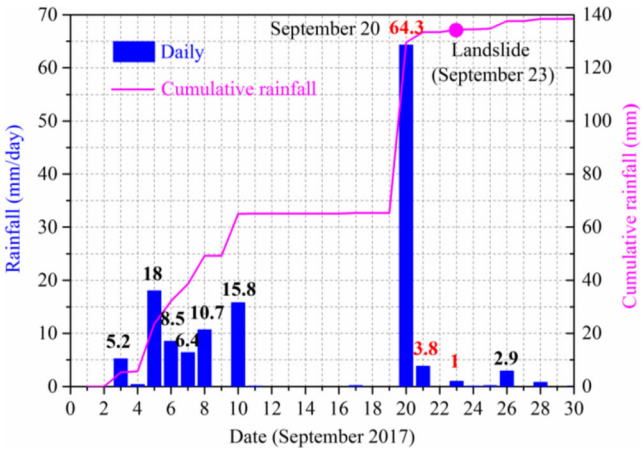

Fig. 6 Rainfall intensity and cumulative rainfall in Libo County in September 2017

carbonate ($CaCO_3$), the main component of limestone, was constantly dissolved to calcium bicarbonate ($Ca(HCO_3)_2$). Then, the $Ca(HCO_3)_2$ entered the developed fissures in the sliding band along with groundwater. In a closed hydrodynamic environment, $Ca(HCO_3)_2$ decomposed easily under normal temperature. Therefore, $CaCO_3$ precipitated and formed calcites parallel to the sliding surface (Fig. 3b). Calcites diminished the integrity of the sliding band and led to the weakening of its mechanical properties. Thus, the rock masses were softened. Then, the shear strength of the sliding surface was reduced, and the sliding force was increased due to the weight of the infiltrating rainwater. The stability of the slope was further deteriorated. Based on the characteristics of the failure mode of the Libo landslide, the failure mode of this landslide is similar to that of a progressive landslide (Yin et al. 2011; Zou 2014; Tang et al. 2015). Under the action of gravity of slope body and erosion action of rainwater, cracks on the top and surface of the slope continued to expand. These provided the appropriate geological conditions for the occurrence of the Libo bedding landslide.

2. The free face formed by the slope excavation was always in an unloading state. Before the landslide, the slope had been accumulating elastic strain energy before the cracks appear. According to the dip angle of the slipping surface (39°) and the mechanical analysis of the Libo bedding rockslide, the maximum shear strain concentrated along the cracks at the front of the slope. As shear strain accumulated, it showed an increase in deformation resulting in the appearance of the lower shear outlet (Fig. 2a). In addition, joint surfaces continued to develop under the shear deformations of the sliding surface and the erosion action of rainwater. The mudstone interlayer in the limestone and the tensile failure of the fracture platform provided convenient conditions for the connection of adjacent sliding surfaces (the step-path failure mode in Fig. 8b). These characteristics provided the potential sliding surface for the landslide.
3. Based on field investigations, all the exposed anchor rods on the sliding bed were cut off by the landslide body. As shown in Fig. 7, only a small part of the anchor rods still embedded in the rock masses. Therefore, their reinforcing effects on the fourth slope grade were limited. Under the erosion action of rainwater and tensile stress of the overlying rock masses of the area II-1 and area II-2, the tension fracture groove at the back edge of the slope continued to develop and eventually cut through. Then, the creeping slip of the overlying rock masses of the area II-1 occurred, and the sliding groove line appeared on the left and right sides. Finally, the tension cracks of the fracture platform between area II-1 and area II-2 cut through (Fig. 8a). Therefore, the slipping surfaces of the area II-1 and area II-2 were connected (Fig. 8b).
4. Under the pushing action of the landslide body and the development of cracks in the lower shear outlet, the elastic strain

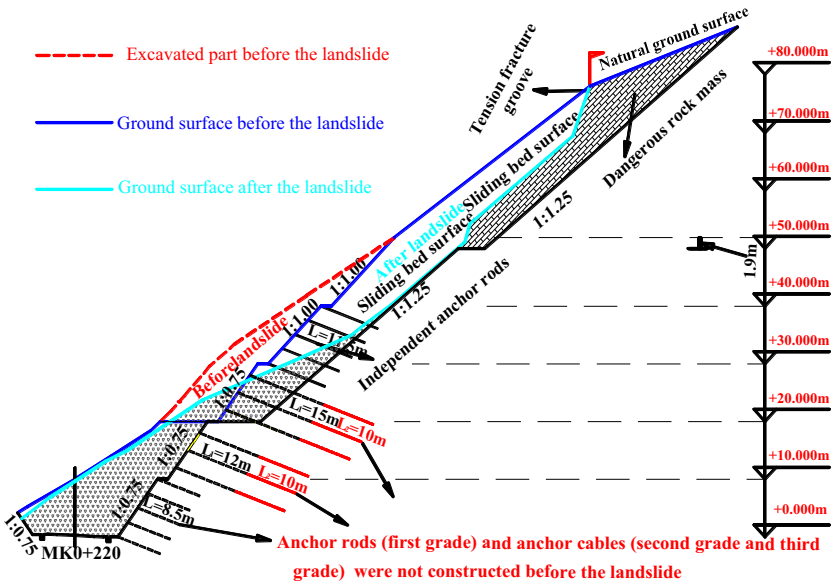

Fig. 7 Slope excavation situation before and after the landslide

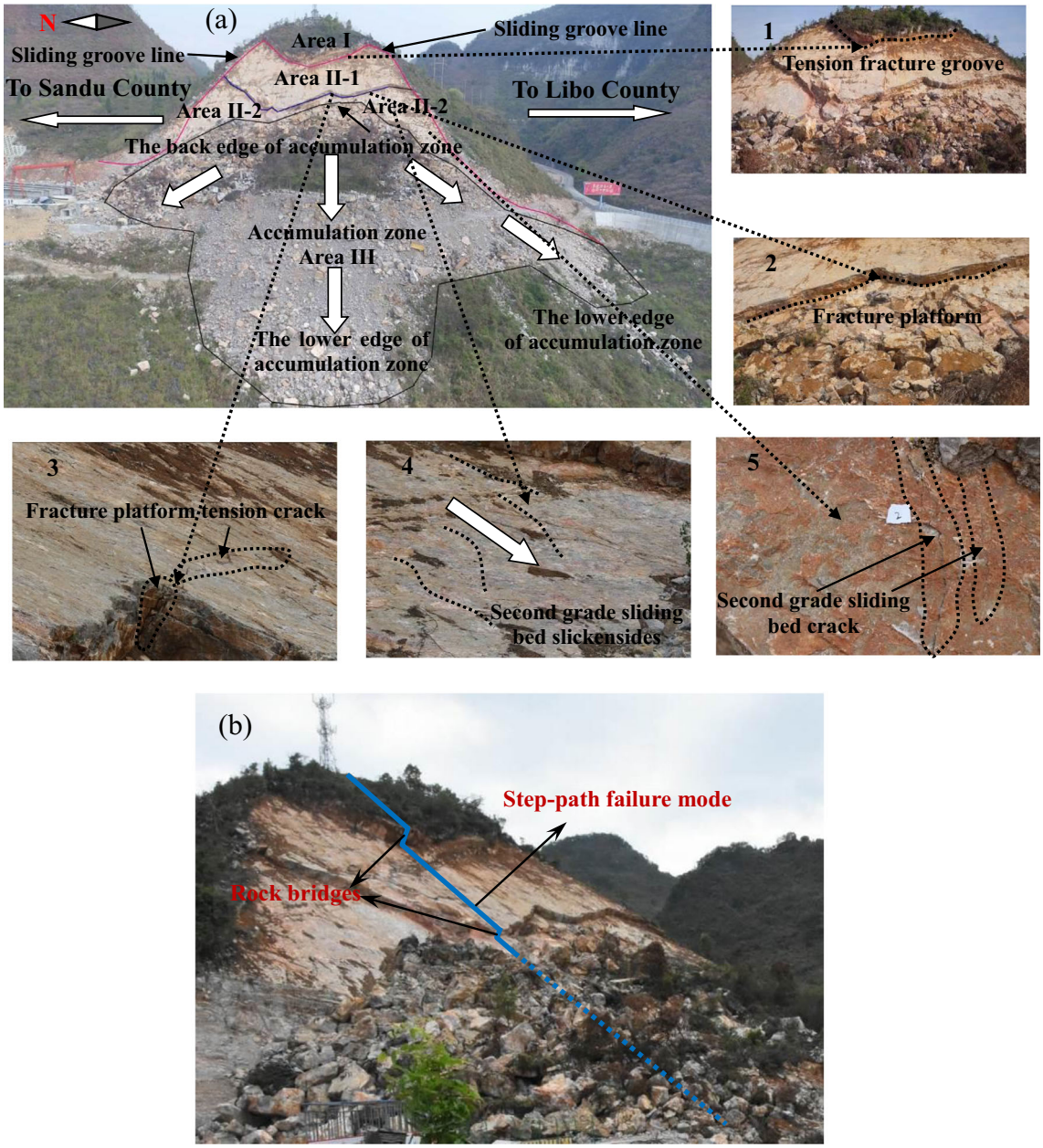

Fig. 8 The division and characteristics of the bedding rockslide. **a** 1 Tension fracture groove (area I); 2 fracture platform (area II); 3 fracture platform tension crack (area II-1); 4 second-grade sliding bed slickensides (area II-2); 5 second-grade sliding bed crack (area II-2). **b** Step-path failure mode

energy accumulated in the slope released rapidly along the direction of crack development and the step-path sliding surface was finally formed. The landslide body slipped in the lower part of the slope. The back edge of the landslide body accumulated in a curved shape at the bottom of the area II-2. The lower edge of the landslide body continued to slip in two directions along the embankment slope (Fig. 8a). Finally, the entire landslide process was completed.>

Discussion

After the landslide, it was found that the upper rock masses (Fig. 9a) was about to slide easily for the following reasons: (1) The integrity of the rock masses was poor; (2) the slope was steep with a dip angle of approximately 39° and had bedding characteristics; (3) a free face was formed after the landslide (Fig. 9b); and (4) evident cracks appeared on the tension fracture groove (Fig. 9b).

For safety, a blasting treatment was carried out on this part of rock masses. The total weight of explosives used in this blasting was 1.72×10^3 kg. There were a total of 15 blasting holes with apertures ranging from 111 to 115 mm. The depth of the blasting holes in the middle position was 18 m, and the depth on both sides was 15 m. The distance from the blasting holes to the free face was approximately 7 m.

It was found that the failure mechanism of the area I was similar to that of the previous bedding rockslide. They have the following similar characteristics:

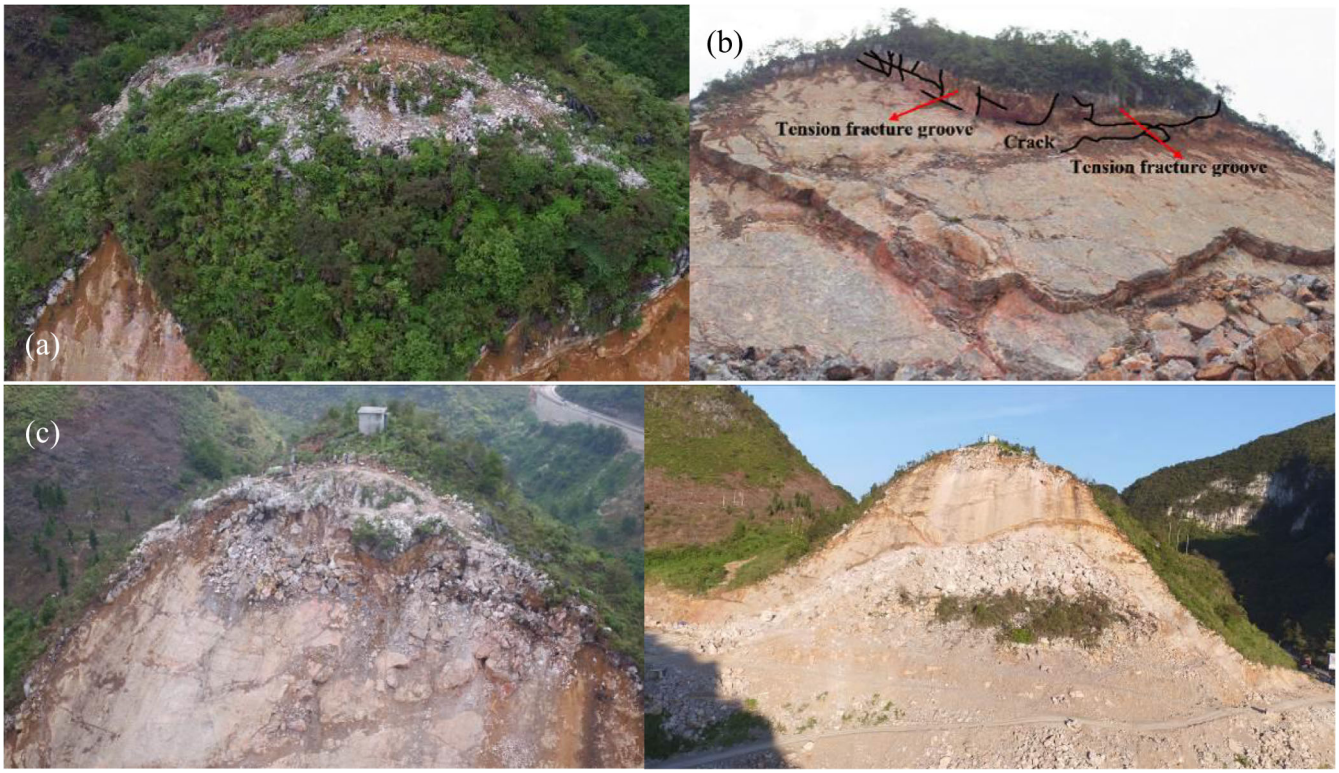

Fig. 9 **a** The upper unstable and dangerous rock masses. **b** The tension fracture groove. **c** The slope after the blasting

Table 1 Attitude of rock formation of the main sections

Number	Position	Attitude of rock formation	Dip direction and dip angle of slope	Remark
1	MK0+120 right 18 m	223° ∠ 30°	220° ∠ 24°	Bedding
2	MK0+220 right 33 m	262° ∠ 43°	255° ∠ 45°	Bedding
3	MK0+250 right 3 m	303° ∠ 21°	262° ∠ 45°	Near bedding
4	MK0+363 right 54 m	281° ∠ 31°	297° ∠ 44°	Bedding
5	MK0+480 right 60 m	280° ∠ 30°	295° ∠ 46°	Bedding

1. They both have free faces. The free face of the bedding rockslide was caused by slope excavation, but the free face of the area I was caused by the landslide body.
2. They have the same bedding joint surface characteristics. The sliding surfaces of the area I and the area II-1 were located on the same joint surface (Fig. 9c). In addition, before the landslides, cracks appeared on the lower part of the two landslide regions.
3. They are induced by external factors. The triggering factor of the previous bedding rockslide was continuous rainfall, while the triggering factor of the area I landslide was artificial blasting.>

In summary, the bedding characteristics, development of the joints, and formation of the free surface provided appropriate conditions for a landslide to occur.

Conclusions

A bedding rockslide occurred at 18:05 (UTC+8) on September 23, 2017, in Libo County, Guizhou Province, China, after 2 days of continuous rainfall. The process of the bedding rockslide was analyzed and the failure mechanism was revealed. The following conclusions are drawn:

The failure mechanism of the bedding rockslide is briefly presented as follows: under the erosion action of rainwater, rock masses and sliding band were softened, and the tension cracks on the top and surface of the slope continued to expand. The existence of the free face caused by slope excavation was responsible for the appearance of cracks in the lower shear outlet. Under the pushing action of the sliding body, the step-path sliding surface cut through owing to the tension failure of the fracture platform. Finally, the landslide masses slipped in the lower part of the slope and the entire landslide process was completed.

The failure mechanism of the blasting landslide was similar to that of the previous bedding rockslide. The bedding characteristics, development of the joints and cracks, steep slope, and formation of the free surface are key factors for the landslide. Therefore, even if this unstable and dangerous rock masses had not been blasted, the bedding landslide was to occur in the rock masses under the other triggering factors (i.e., continuous rainfall, slope excavation, and/or earthquakes).

Funding information

This study was financially supported by the National Natural Science Foundation of China (Nos. 51478477 and 51878668), the Guizhou Provincial Department of Transportation Foundation (Nos. 2014122006 and 2017122058), the program of China Scholarship Council, and the Fundamental Research Funds for the Central Universities of Central South University (No. 2017zzts199). All financial supports are greatly appreciated.

References

Cen DF, Huang D, Ren F (2017) Shear deformation and strength of the interphase between the soil-rock mixture and the benched bedrock slope surface. Acta Geotech 12(2):391–413

Cogan J, Gratchev I, Wang GH (2018) Rainfall-induced shallow landslides caused by ex-Tropical Cyclone Debbie, 31st March 2017. Landslides 15(6):1215–1221

Gu DM, Huang D, Yang WD, Zhu JL, Fu GY (2017) Understanding the triggering mechanism and possible kinematic evolution of a reactivated landslide in the Three Gorges reservoir. Landslides 14(6):2073–2087

Huang RQ, Pei XJ, Cui SH (2016) Cataclastic characteristics and formation mechanism of rock mass in sliding zone of Daguangbao landslide. Chin J Rock Mech Eng 35(1):1–15

Huang D, Gu DM, Song YX, Cen DF, Zeng B (2018) Towards a complete understanding of the triggering mechanism of a large reactivated landslide in the Three Gorges Reservoir. Eng Geol 238:36–51

Li WC, Dai FC, Wei YQ, Wang ML, Min H, Lee LM (2016) Implication of subsurface flow on rainfall-induced landslide: a case study. Landslides 13(5):1109–1123

Lin F, Wu LZ, Huang RQ, Zhang H (2018) Formation and characteristics of the Xiaoba landslide in Fuquan, Guizhou, China. Landslides 15(4):669–681

Ouyang CJ, Zhou KQ, Xu Q, Yin JH, Peng DL, Wang DP, Li WL (2017) Dynamic analysis and numerical modeling of the 2015 catastrophic landslide of the construction waste landfill at Guangming, Shenzhen, China. Landslides 14(2):705–718

Regmi AD, Yoshida K, Cui P, Hatano N (2017) Development of Taprang landslide, West Nepal. Landslides 14(3):929–946

Tang HM, Zou ZX, Xiong CR, Wu YP, Hu XL, Wang LQ, Lu S, Criss RE, Li CD (2015) An evolution model of large consequent bedding rockslides, with particular reference to the Jiweishan rockslide in Southwest China. Eng Geol 186:17–27

Tang GP, Huang JS, Sheng DC, Sloan SW (2018) Stability analysis of unsaturated soil slopes under random rainfall patterns. Eng Geol 245:322–332

Wang YS, Zhao B, Li J (2017) Mechanism of the catastrophic June 2017 landslide at Xinmo Village, Songping River, Sichuan Province, China. Landslides 14(4):333–345

Xue DM, Li TB, Zhang S, Ma CC, Gao MB, Liu J (2018) Failure mechanism and stabilization of a basalt rock slide with weak layers. Eng Geol 233:213–224

Yin YP, Sun P, Zhang M, Li B (2011) Mechanism on apparent dip sliding of oblique inclined bedding rockslide at Jiweishan, Chongqing, China. Landslides 8(1):49–65

Zhang LL, Zhang J, Zhang LM, Tang WH (2011) Stability analysis of rainfall-induced slope failure: a review. Geotech Eng 164(5):299–316

Zhang LL, Li JH, Li X, Zhang J, Zhu H (2016) Rainfall induced soil slope failure: stability analysis and probabilistic assessment. CRC Press 20(1):19–24

Zhao LH, Zuo S, Lin YL, Li L, Zhang YB (2016) Reliability back analysis of shear strength parameters of landslide with three-dimensional upper bound limit analysis theory. Landslides 13(4):711–724

Zhao LH, Zuo S, Deng DP, Han Z, Zhao B (2018) Development mechanism and parameter inversion analysis for landslides: a case study of the landslide at Xinlu Village, Chongqing, China. Landslides 15(10):2075–2081

Zou ZX (2014) Research on evolution dynamics of the consequent bedding rockslides [D]. China Univ Geosci

L. Zhao · D. Li · X. Cheng · S. Zuo (✉)
School of Civil Engineering,
Central South University,
Changsha, 410075, Hunan, China
Email: zuoshi@csu.edu.cn

L. Zhao
Key Laboratory of Heavy-Haul Railway Engineering Structure, Ministry of Education,
Central South University,
Changsha, 410075, Hunan, China

D. Li (✉) · X. Cheng
Faculty of Arts and Science,
Kyushu University,
Fukuoka, 8190395, Japan
Email: 134812167@csu.edu.cn

H. Tan
Guizhou Province Quality and Safety Traffic Engineering Monitoring and Inspection Center Co., Ltd.,
Guiyang, 550081, Guizhou, China